Chapter 2. New observational diagnostics of solar, stellar and interstellar magnetic fields

Luis Campusano

Diagnosing coronal magnetic fields with radio imaging-spectroscopy technique

Yihua Yan[1,2] , **Baolin Tan**[1,2], **V. Melnikov**[1,3], **Xingyao Chen**[1],
Wei Wang[1], **Linjie Chen**[1], **Fei Liu**[1] **and MUSER Team**[1]

[1]CAS Key Lab of Solar Activity, National Astronomical Observatories,
Chinese Academy of Sciences, Beijing 100101, China
email: yyh@nao.cas.cn

[2]School of Astronomy & Space Science, University of Chinese Academy of Science,
Beijing, China

[3]Pulkovo Observatory of Russian Academy of Sciences, Saint Petersburg, Russia

Abstract. Mingantu Spectral Radioheliograph (MUSER) is an aperture-synthesis imaging telescope, dedicated to observe the Sun, operating on multiple frequencies in dm to cm range. The ability of MUSER to get images and measure Stokes I and V parameters simultaneously at many frequencies in a wide band is of fundamental importance. It allows one to approach/solve such important problems as measuring the strength, geometry and dynamics of magnetic field at coronal heights. Here we consider some of the recently developed radio physics methods to be used for solving the problems. These methods allow us to obtain information that is unattainable in other areas of the electromagnetic spectrum.

Keywords. Sun: magnetic fields, Sun: corona, Sun: radio radiation, Sun: flares, Sun: coronal mass ejections (CMEs)

1. Introduction

Radio dynamic imaging spectroscopy is important to understand the primary energy release process, particle accelerations and propagations. The radio FS locations are mostly not clear. The emission mechanism corresponding to different regions in the solar corona is in general different: bremsstrahlung emission in the quiet corona; cyclotron (gyro-resonance) and gyro-synchrotron emission in the active regions; and synchrotron, plasma emission, and/or electron cyclotron maser in the flaring regions. Therefore, the coronal magnetic field diagnostics is a most complicated work including determining exactly physical partitions in source regions, identifying emission mechanism, applying diagnosing functions, etc. The free parameters need to be specified in order to diagnose coronal magnetic fields(Casini *et al.* (2017)).

Either solar or non-solar dedicated new facilities, e.g., JVLA, ALMA, LOFAR, MWA, MUSER, SRH, GRH, etc., have been developed to make progress in addressing these solar radio problems (Ramesh *et al.* (1998); Yan *et al.* (2009); Lesovoi *et al.* (2012); Chen *et al.* (2013, 2015); Shimojo *et al.* (2017); Reid & Kontar (2017); Kontar *et al.* (2017); Mohan & Oberoi (2017); Chen *et al.* (2019)).

In the next section, we will present the diagnosing methods for coronal magnetic fields with radio observations. Then we introduce the initial observations of Mingantu Spectral Radioheliograph (MUSER), which is expecting to make progress for diagnosing coronal magnetic fields.
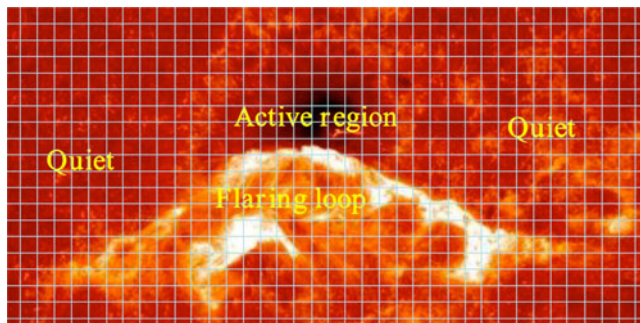
Figure 1. Different regions correspond to different emission mechanisms.

2. Diagnosing Coronal Magnetic Fields by Radio Techniques

The imaging-spectroscopy ability of MUSER (Yan *et al.* (2009)) allows to approach/ solve such important problems such as: measuring the strength, geometry and dynamics of magnetic field at coronal heights; identifying triggers of solar flares and CMEs; and selecting the most appropriate mechanism/model of electron acceleration in solar flares, as shown in in Fig. 1. Factors to diagnose coronal magnetic fields are discussed in a recent review of coronal magnetic field diagnostics by Casini *et al.* (2017).

The observed radio parameters include: frequency, intensity, polarization, duration, and drift rate, etc. The diagnosing functions correspond to the different emission mechanism. The Corona magnetic fields will be obtained in terms of the strength, the direction and the location.

Different region may correspond to different mechanism. Exactly physical partition, and the corresponding diagnosing functions are the key factors to obtain coronal magnetic fields.

Quiet solar corona: The bremsstrahlung emission may be applied to weak field. The coronal B_l can be measured from the difference of free-free absorption coefficients between O-mode and X-mode emission by measuring the polarization degree (P) and spectral index (δ) (Gelfreikh *et al.* (1987); Gelfreikh (2004)):

$$B_l \approx \frac{10714}{\lambda \delta} \ P, \quad (\text{unit} : \text{Gs}), \quad P = \frac{T_b^R - T_b^L}{T_b^R + T_b^L}, \delta = -\frac{\partial \log T_b}{\partial \log f} = \frac{\partial \log T_b}{\partial \log \lambda}.$$

When the source region is optical thin, $\delta \sim 2$, then

$$B_l \approx \frac{5357}{\lambda} P,$$

where the unit of the magnetic field B_l is Gs, and that of the wavelength λ is cm.

The sensitivity mainly depends on the accuracy of polarization measurements. The applications can be found in Zhang *et al.* (2002) and Iwai *et al.* (2014).

Above active region: The cyclotron (gyro-resonance) & gyro-synchrotron emission can be applied to the active regions or the network magnetic regions with strong field.

The edges where the optically thick layer drops below the transition region can be identified by the rapid drop in the brightness temperature. From the ratio of the edge frequencies in the two modes, the harmonic numbers of the corresponding gyroresonance layers can be identified, and the magnetic field B can also be identified unambiguously (White *et al.* (1991)).

Zhou & Karlicky (1994) obtained a set of modified expressions of coronal magnetic fields after Dulk & Marsh (1982) with

$$B \approx \left[\frac{c^2}{kT_{br}A_1} f_{pk}^{1.3+0.98\delta} f^{-0.78-0.9\delta} A_2^{-2.52-0.08\delta} \right]^{\frac{1}{0.52+0.08\delta}},$$

$$A_1 \approx 4.24 \times 10^{14+0.3\delta}(\sin\theta)^{0.34+0.07\delta} , \quad A_2 \approx 2.8 \times 10^6,$$

where c is the speed of light, f_{pk} is the peak frequency, δ is the spectral index, T_b is the brightness temperature, and $2 < \delta < 7$, $10 < \text{harmonics } (s) < 100$, $E_0 > 10$ keV for simple source. The magnetograms derived from 17 GHz of NoRH was presented in Huang (2006).

Recently Fleishman & Kuznetsov (2010) developed fast GS codes with sufficient accuracy, and applicable to both isotropic and anisotropic electron distributions. Computation time for the exact formulae grows exponentially with the harmonic number, while for the fast algorithm this is nearly constant. The codes are freely available for use, and are incorporated into SSW.

Flaring region: The gyrosynchrotron, plasma emission, or electron cyclotron maser mechanism (ECME) can be applied to the flaring source regions with strong field and fast changing processes. For the flaring source regions, it is highly dynamic, including plasma instabilities, particle accelerations, and fast energy releases.

Radio spectral fine structures, e.g., microwave quasi-periodic pulsations (QPP), zebra patterns, Type III pairs, fiber bursts, etc., are the indicators of flaring source regions and the coronal magnetic field can be diagnosed.

For the observed microwave QPP structures (Tan *et al.* (2010)), if they are from fast sausage oscillation modes, one can have the period P related to the magnetic field B as follows:

$$P_{sausage}^{fast} \approx 2.02 \times 10^{-16} \frac{a\sqrt{n_e}}{B}$$

and if they are from due to the fast kink oscillation modes, one obtains the relation between the period P and the magnetic field B as follows:

$$P_{kink}^{fast} \approx 6.48 \times 10^{-17} \frac{L\sqrt{n_e}}{B}$$

where a is the section radius, L is the loop length, and n_e is the plasma density.

For the observed fiber burst structures, the magnetic field can be derived as follows (Wang & Zhong (2006)),

$$B = \frac{4\pi H_n \sqrt{m_i m_e}}{ec} \frac{df}{dt} \approx 10.15 \times 10^{-14} H_n \frac{df}{dt}, \quad (\text{Gs})$$

where m_i, m_e are ion and electron mass, respectively, e is the electron charge, c is the speed of light, H_n is the density scale height, and f is the frequency.

According to the physical classification (Tan *et al.* (2014)), different types of zebra pattern (ZP) structures may be due to different coupling processes. Therefore, we should adopt different mechanism to derive the magnetic fields in source regions:

(1) Bernstein model (Zheleznyakov & Zlotnik (1975)):

$$B \approx \frac{2\pi m_e}{e} \Delta f;$$

(2) Whistle Wave model (Chernov (1996); Chernov *et al.* ((2005)):

$$B \approx 71.1 \times 10^{-8} \Delta f;$$

(3) Double plasma layer resonance (DPR) model (Zheleznyakov & Zlotnik (1975)):

$$B \approx 35.6 \times 10^{-8} \frac{2H_n - H_b}{H_b} \Delta f.$$

In the above, Δf is the frequency difference between the adjacent zebra strips and H_n, H_b are scale heights of the density and the magnetic field, respectively.

For the ZPs observed in an X2.2 flare event on 15 Februry 2011, the magnetic field decreases obviously from the flare rising phase to its decay phase (Tan *et al.* (2012)). The relaxation of magnetic field relative to plasma density was also found as revealed from microwave ZPs (Yan *et al.* (2007), Yu *et al.* (2012))

For the microwave Type III pairs (Tan *et al.* (2016)), the plasma density around source region is obtained from the separation regime of the opposite frequency drifting directions as $n_x = \frac{f_x^2}{81s^2}$, m^{-3}, where s is the harmonic number, The temperature T can be derived from the ratio of SXR emission fluxes at two energy bands. Then the magnetic field B is obtained as:

$$B \approx (B_L + B_H)/2,$$

$$B_L > 3.402 \times 10^{-19} (n_x T \bar{D} R_c)^{1/2} , \quad B_H < 3.293 \times 10^{-16} \left[\frac{n_x T \bar{D} R_c}{(n_x \tau)^{1/3}} \right]^{1/2} ,$$

with B_L and B_H as the magnetic field corresponding to the normal and RS type III branches, respectively. The beam velocity can be obtained as

$$v_b \approx \frac{2\mu_0 n_x k_B T}{B^2} \bar{D} R_c.$$

The length of the acceleration regions can be estimated as

$$L_c = \frac{\mu_0 n_x k_B T}{B^2} R_c \frac{\Delta f}{f_x}.$$

In the above, R_c is the curvature radius of the magnetic field lines, τ is the burst lifetime defined as the time difference between the start and end of each individual type III burst, μ is the magnetic permeability, k_B is the Boltzmann constant, $\bar{D}$ is the relative frequency drift rate and Δf is the the observed frequency gap between the normal and RS type III branches.

For the Type-III pairs observed in a flare event on 26 September 2011 as shown in Fig. 2(a) (Tan *et al.* (2016)), the observed parameters are as follows. For normal branches, the frequency drift rate is 2.12–7.38 GHz/s. The relative frequency drift rate is 1.52–5.06 s^{-1}. The separate frequency is in 1.22–1.49 GHz and the frequency gap is in 172–442 MHz. For RS branches, the frequency drift rate is 281–647 MHz/s. The relative frequency drift rate is 0.23-0.50 s^{-1}. We can derive the diagnosed results as shown in Fig. 2(b). It can be seen that the plasma $\beta > 1$, which means that it is highly dynamic and unstable near the source region. Although RS branches drift about 10 times slower than the normal branches, the energies of upward electrons are still close to the downward electrons. Both of the upward and downward electrons are possibly accelerated by similar mechanism (Tan *et al.* (2016)).

3. MUSER Progress and Initial Observations

MUSER is a solar-dedicated imaging-spectroscopy facility with its brief specification as shown in Table 1 (Yan *et al.* (2009)). MUSER data is processed using CASA and some own developed programs-Direct FT. They have made all code available at https://github.com/astroitlab/museros (Mei *et al.* (2018)). During 2014-2019, a total number of 83 solar radio burst events have been registered by MUSER, as shown in Table 2.

Table 1. Brief Specifications of MUSER.

Array	MUSER-I	MUSER-II
Frequency range	0.4 - 2 GHz	2 - 15 GHz
Antennas	40(Φ4.5 m)	60 (Φ2 m)
Frequency channel	64 (25 MHz)	520 (25 MHz)
Space resolution	$51.6'' - 10.3''$	$10.3'' - 1.4''$
Time resolution	$\sim$25 ms	$\sim$200 ms
Polarizations	LCP, RCP	LCP, RCP
Maximum baseline	$\sim$3 km	$\sim$3 km

Table 2. Event list of MUSER in 2014-2019.

Flare class	Number of radio burst events
X	2
M	15
C	38
B	19
A	4
below A	5
Total number	83

The observed Type III paris.

The diagnosed parameters.
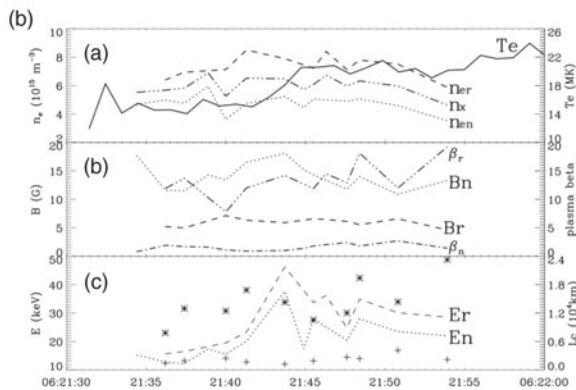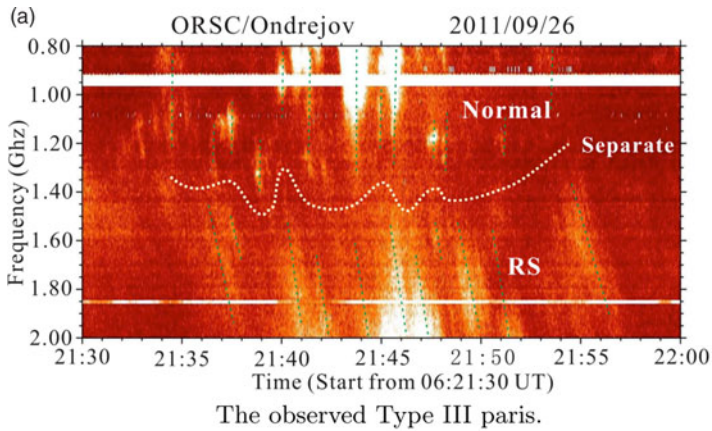
Figure 2. The Type-III pairs observed in a flare event on 26 September 2011 and the diagnosed results (Tan *et al.* (2016)).
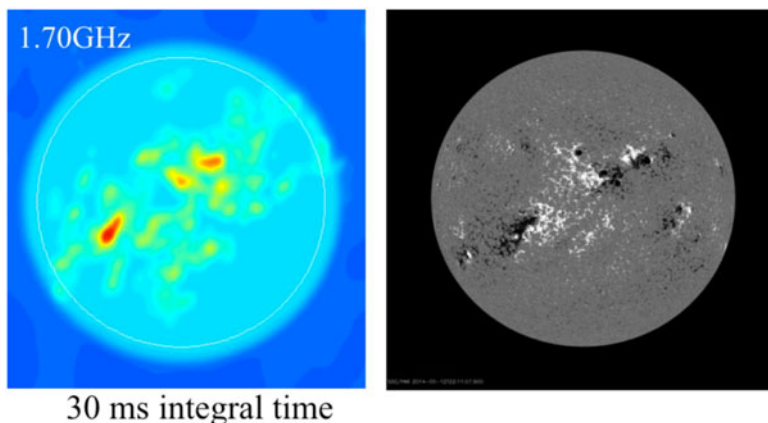
Figure 3. Radio intensity image (*left panel*) of the quiet Sun observations on 12 May 2014 by MUSER and the full disk HMI/SDO magnetogram (*right panel*).

Fig. 3 shows the radio intensity image of the quiet Sun observations on 12 May 2014 by MUSER and the full disk magnetogram of the line of sight component of the photospheric magnetic field by HMI/SDO. It can be seen that the radio features agree with the magnetic field properly. Further data processing is needed for future studies to obtain coronal magnetic fields from observed data based on the above methods.

4. Summary

In summary, solar radio approaches for diagnosing coronal magnetic fields have been developed for quiet Sun, active regions and flaring processes. The imaging-spectroscopy observations are needed for radio fine structure analyses. MUSER progress and observations are promising and further data processing is needed for future studies.

Acknowledgements

References

Casini, R., White, S. M., & Judge, P. G. 2017, *Space Sci. Rev.*, 210, 145

Chen, B., Bastian, T. S., Shen, Chengcai, Gary, D. E., Krucker, S., & Glesener, L. 2015, *Science*, 350, 1238

Chen, B., Bastian, T. S., White, S. M., Gary, D. E., Perley, R., Rupen, M., & Carlson, B. 2013, *ApJ*, 763, 21

Chen, B., Shen, C., Reeves, K. K., Guo, F., & Yu, S. 2019, *ApJ*, 884, 63

Chernov, G. P. 1996, *Astronomy Reports*, 40, 561

Chernov, G. P., Yan, Y. H., Fu, Q. J., & Tan, Ch. M. 2005, *A&A*, 437, 1047

Dulk, G. A. & Marsh, K. A. 1982, *ApJ*, 259, 350

Fleishman, G. D. & Kuznetsov, A. A. 2010, *ApJ*, 721, 1127

Gelfreikh, G. B. 2004, in: Gary D.E., Keller C.U. (eds) *Solar and Space Weather Radiophysics. Astrophysics and Space Science Library*(Dordrecht: Springer), vol. 314, p.115

Gelfreikh, G. B., Peterova, N. G., & Riabov, B. I. 1987, *Sol. Phys.* 108, 89

Huang, G. 2006, *Sol. Phys.*, 237, 173

Iwai, K., Shibasaki, K., Nozawa, S., Takahashi, T., Sawada, S., Kitagawa, J., Miyawaki, S., & Kashiwagi, H. 2014, *Earth Planets & Space*, 66, 149

Kontar, E. P., Yu, S., Kuznetsov, A. A., Emslie, A. G., Alcock, B., Jeffrey, N. L. S., Melnik, V. N., Bian, N. H., & Subramanian, P. 2017, *Nature Comm.*, 8, 1515

Lesovoi, S. V., Altyntsev, A. T., Ivanov, E. F., & Gubin, A. V. 2012, *Sol. Phys.*, 292, 168

Mei, Y., Wang, F., Wang, W., Chen, L. J., Liu, Y. B., Deng, H., Dai, W., Liu, C. Y., & Yan, Y. H. 2018, *PASP*, 130, 14503

Mohan, A. & Oberoi, D. 2017, *Sol. Phys.*, 292, 168

Ramesh, R., Subramanian, K. R., Sundararajan, M. S., & Sastry, Ch. V. 1998, *Sol. Phys.*, 181, 439

Reid, H. A. S. & Kontar, E. P. 2017, *A&A*, 606, 141

Shimojo, M., Bastian, T. S., Hales, A. S., *et al.* 2017, *Sol. Phys.*, 292, 87

Tan, B. L., Karlický, M., Mészárosová, H., Kashapova, L., Huang, J., Yan, Y., & Kontar, E. P. 2016, *Sol. Phys.*, 291, 2407

Tan, B. L., Tan, C. M., Zhang, Y., Mészárosová, H., & Karlický, M. 2014, *ApJ*, 780, 129

Tan, B. L., Yan, Y., Tan, C. M., Sych, R., & Gao G. N. 2012, *ApJ*, 744, 166

Tan, B. L., Zhang, Y., Tan, C. M., & Liu Y. Y. 2010, *ApJ*, 723, 25

Wang, S. J. & Zhong, X. C. 2006, *Sol. Phys.*, 236,155

White, S. M., Kundu, M. R., & Gopalswamy, N. 1991, *ApJ*, 366, 43

Yan, Y. H., Huang, J., Chen, B., & Sakurai, T. 2007, *PASJ*, 59, 815

Yan, Y. H., Zhang, J., Wang, W., Liu, F., Chen, Z. J., & Ji, G. 2009, *Earth Moon Planets*, 104, 97

Yu, S. J., Yan, Y. H., & Tan, B. L. 2012, *ApJ*, 761, 136

Zhang, C.-X., Gelfreikh, G. B., & Wang, J.-X. 2002, *Chin. J. Astron. Astrophys.*, 2, 266

Zhelezniakov, V. V. & Zlotnik, E. Ia. 1975a, *Sol. Phys.*, 43, 431

Zhelezniakov, V. V. & Zlotnik, E. Ia. 1975b, *Sol. Phys.*, 44, 461

Zhou, A. H. & Karlicky, M. 1994, *Sol. Phys.*, 153, 441

Discussion

IRINA KITIASHVILI: You detected high plasma-β in the solar corona. Could you, please, describe how for this region located above photosphere and how it evolves?

YIHUA YAN: The region corresponds to the frequency regime of 1.22 GHz – 1.49 GHz, which correspond to the plasma density of about 6.0×10^{15} m^{-3} (with harmonics s= 2). Therefore this region located about 8000 km – 40000 km above the photosphere. It evolves dynamically during about 20 second period, e.g., as shown in Fig. 2(b) (for details, please refer to Tan *et al.* 2016).